

# Supporting Information: Criticality of Symmetry in Rational Design of Chalcogenide Perovskites

*A. Nijamudheen and Alexey V. Akimov\**

Department of Chemistry, University at Buffalo, The State University of New York, Buffalo,  
NY 14260-3000

\*Corresponding author. Email: [alexeyak@buffalo.edu](mailto:alexeyak@buffalo.edu)

## **S1. Details of the computational methodology**

The crystal structures of the studied systems are refined by a variable-cell optimization of the initial guess structures (selected based on the experimental studies of BaZrS<sub>3</sub> (BZS) structure<sup>1,2</sup>) using DFT. The electronic exchange and correlation are described by using the PBE functional.<sup>3</sup> The core electrons are accounted for implicitly via the PAW atomic pseudopotentials, whereas the plane waves are used to describe the valence electrons. For the geometry optimizations and the DOS calculations, a plane wave cutoff of 45 Ry and a density cutoff of 350 Ry are used, while the Brillouin zone is sampled using a 7×4×5 k-point mesh. All electronic structure calculations, ground state MD simulations, and phonon calculation have been performed using the Quantum Espresso package.<sup>4</sup> We have computed the infrared (IR) active phonon modes of the simplest unit cell of BZS at the  $\Gamma$  point. A 3×3×2 k-point mesh is used for the optimization of this unit cell and for the self-consistent calculation to produce the wave-function required the

phonon calculations. The absence of any imaginary frequencies verifies BZS as a minimum in the potential energy surface.

Ground state molecular dynamics (MD) trajectories of 3.2-3.5 ps length have been computed using velocity Verlet integration scheme with the time steps of 1 fs. The ground state MD trajectories are used to perform non-adiabatic coupling (NAC) calculations and subsequent NA-MD simulations. For the ground state MD simulation, we sample the Brillouin zone by a  $3 \times 2 \times 2$  k-point mesh. Initial benchmarking shows that the use of  $3 \times 2 \times 2$  k-point mesh can produce reasonably accurate geometries and energies for the perovskite unit cells compared to the calculations using a denser  $7 \times 4 \times 5$  k-point mesh (the details are given in the section 8 of SI). It significantly improves the geometries and energies compared to the use of only  $\Gamma$  point for producing MD trajectory. The present approach based on plane-wave DFT and a reasonably dense k-point mesh for Brillouin-zone sampling is suitable for describing the vibrational properties of the system.<sup>5-8</sup> The PBE+U method is employed for calculating the NAC between the frontier molecular orbitals. Hybrid HSE06<sup>9</sup> level calculations are performed to validate the bandgaps and DOSs computed using the PBE+U approximation.<sup>10,11</sup> Only the  $\Gamma$  point is used in the NAC calculations. This do not affect the NAC significantly because all the systems that we discuss here have direct bandgaps at  $\Gamma$  point.

At every time step of the MD trajectory, the NAC ( $\vec{d}_{ij}$ ) between the Kohn-Sham orbitals are computed numerically by employing the methodology developed by Hammes-Schiffer and Tully<sup>12</sup> (eq. S1).

$$\vec{d}_{ij}\left(t+\frac{dt}{2}\right)=\frac{1}{2dt}\left[\left\langle\phi_i\left(\vec{r};\vec{R}(t)\right)\left|\phi_j\left(\vec{r};\vec{R}(t+dt)\right)\right\rangle-\left\langle\phi_i\left(\vec{r};\vec{R}(t+dt)\right)\left|\phi_j\left(\vec{r};\vec{R}(t)\right)\right\rangle\right]. \quad (\text{S1})$$

In eq. 1,  $\phi_i(\vec{r}; \vec{R}(t))$  represents the KS orbital with index  $i$  at time  $t$ ;  $\vec{r}$  and  $\vec{R}(t)$  are the electronic and nuclear coordinates, respectively.

NAC calculations and quantum-classical, non-adiabatic molecular dynamics (NA-MD) simulations are performed by using the PYXAID package.<sup>13,14</sup> The Boltzmann averaged NAC is calculated as,

$$\frac{\sum_{j,k} \langle NAC \rangle_{jk} e^{\frac{-\Delta E_{jk}}{K_B T}}}{\sum_{j,k} e^{\frac{-\Delta E_{jk}}{K_B T}}}, \quad (\text{S2})$$

where  $\langle NAC \rangle_{jk}$  represents the NAC averaged over all time steps of the MD trajectory coupling the states  $j$  and  $k$ ,  $\Delta E_{jk}$  is energy gap between the states  $j$  and  $k$ .  $K_B$  and  $T$  are the Boltzmann constant and the simulation temperature (300 K), respectively.  $j$  and  $k$  represent the indices of occupied and unoccupied orbitals, respectively, which are included in the active space used for the NA-MD simulations.

Similarly, the Boltzmann averaged dephasing times are computed using the formula,

$$\frac{\sum_{j,k} \langle Deph \rangle_{jk} e^{\frac{-\Delta E_{jk}}{K_B T}}}{\sum_{j,k} e^{\frac{-\Delta E_{jk}}{K_B T}}}, \quad (\text{S3})$$

where  $\langle Deph \rangle_{jk}$  represents the average dephasing time for a transition from state  $j$  to  $k$ .

The variance in NAC between two states  $j$  and  $k$  is calculated using the formula,

$$\langle Variance \rangle_{jk} = \frac{\sum_{t=0}^N (\langle NAC \rangle_{jk} - d_{jk}(t))^2}{N}, \quad (\text{S4})$$

where  $N$  ( $= 3000$ ) represents the length of MD trajectory and  $d_{jk}(t)$  represents the nonadiabatic coupling between the states  $j$  and  $k$  at time  $t$ . Variance in average NAC between all states included in the active space are averaged using a Boltzmann factor using a formula similar to equations (S2-S3). The Boltzmann averaged variance in NAC is presented in the Table 1 of the manuscript.

For NA-MD calculations,  $\sim 3.2$  ps trajectories with 1 fs electronic and nuclear integration time steps are utilized. From the ground-state MD trajectories, 20 initial configurations of  $\sim 3.0$  ps length trajectories are selected for performing NA-MD simulations. Starting from each of the initial configurations, 10000 stochastic surface hopping probabilities are realized. In this study, we utilize the computationally efficient classical path approximation (CPA).<sup>15</sup> The evolution of nuclear coordinates is computed by the ground state MD calculations. The evolution of electron dynamics depends only parametrically on the time dependent ground state nuclear coordinates via the evolution of electronic Hamiltonian and NAC. We assume the neglect of back reaction (NBR); therefore, the evolution of nuclear trajectories is unaffected by the electronic transitions. CPA and NBR are excellent approximations for the condensed matter and solid state systems that have rigid geometrical features and contain a large number of electrons.<sup>16-21</sup> According to the surface hopping methods used, the stochastic probability for an electron to hop from state  $f$  to state  $i$  is accepted by the condition described in eq (5), without any velocity rescaling.<sup>22</sup>

$$P_{acc} = \min \left\{ 1, \exp \left( - \frac{E_f - E_i}{k_B T} \right) \right\}. \quad (\text{S5})$$

In eq. (5),  $E_f$  and  $E_i$  represent the final and initial electronic state energies, respectively,  $T$  denotes the system temperature (set to 300 K), and  $K_B$  is the Boltzmann constant. The time evolution of populations for all states are averaged over all initial configurations and stochastic

SH trajectories. For the NA-MD calculations, bandgaps from  $\Gamma$  point calculations are corrected by means of a scissor operator method.<sup>23–25</sup> More details on the theory and applications of quantum-classical NA-MD simulation and SH methods can be found elsewhere.<sup>15,26</sup>

The original fewest switches surface hopping (FSSH) method is known to incorrectly preserve non-negligible electronic coherence between substantially separated nuclear wave-packets.<sup>22</sup> FSSH may lead to overcoherence and predict faster timescales for electronic transitions. Here, the overcoherence problem of FSSH is accounted for by the decoherence induced surface hopping (DISH) method.<sup>22,27</sup> The DISH methodology is based on an optical response formalism, and is derived from the autocorrelation function of the energy levels of electronic basis states involved in an electronic transition.<sup>28</sup>

Unnormalized autocorrelation function (u-ACF),  $C_{ij}(t)$  for the fluctuation of the energy gap  $E_{ij}(t)$  between states  $i$  and  $j$  as a function of time  $t$  may be calculated from eq. (6).

$$C_{ij}(t) = \langle \delta E_{ij}(t) \delta E_{ij}(0) \rangle. \quad (\text{S6})$$

$$\text{In eq. (6), } \delta E_{ij}(t) = E_{ij}(t) - \langle E_{ij} \rangle. \quad (\text{S7})$$

$\delta E_{ij}(t)$  is defined as the fluctuation in energy gap  $E_{ij}$  from its average value  $\langle E_{ij} \rangle$  along the trajectory. Normalized ACF (n-ACF)  $\tilde{C}_{ij}(t)$  is obtained from  $C_{ij}(t)$  using the expression

$$\tilde{C}_{ij}(t) = \frac{C_{ij}(t)}{\langle \delta E_{ij}^2 \rangle} = \frac{\langle \delta E_{ij}(t) \delta E_{ij}(0) \rangle}{\langle \delta E_{ij}^2 \rangle} \quad (\text{S8})$$

Fourier transform of the normalized autocorrelation function gives the phonon modes associated with a specific electronic transition. The pure dephasing function is calculated from the second order cumulant expansion of an optical response function, as defined elsewhere.<sup>27</sup>

## S2. Details of optimized perovskite geometries

**Table S1.** The lattice parameters (Angstrom) for the optimized supercells for the doped and undoped perovskites. Experimentally measured<sup>2</sup> lattice parameters (Angstrom) are given in the parentheses.

System	a	b	c
BZS	7.04 (7.04)	14.34 (14.10)	10.06 (9.98)
BZTS (12.5%)	7.02	14.23	10.04
BZTS (25%)	6.98	14.13	10.08
BZHS (12.5%)	7.04	14.32	10.04
BZHS (25%)	7.04	14.30	10.04
BZSO	6.29	12.50	10.43
BZSSe	7.25	14.94	10.01

## S3. Bandgaps from different levels of theory and the details of the DFT+U methodology

Our DFT+U and hybrid-DFT calculations predict direct bandgaps of 1.78 and 1.81 eV, respectively for BZS, which are in good agreement with the previously reported bandgaps (~1.8 eV) (Table 2). PBE underestimates the bandgap significantly, and hence not used for further NAC and NA-MD calculations. Although HSE06 accurately reproduces the bandgap for BZS and shows improved values over the PBE for all systems, it also significantly overestimates the bandgaps for some of the doped systems compared to the previous theoretical or experimental reports. Also, it is computationally expensive to use HSE06 for performing MD and NAC calculations. Therefore, PBE+U was used to accurately reproduce the gaps for all systems.

Unless noted otherwise, all DOS, NAC, and NA-MD data discussed are from PBE+U calculations.

**Table S2.** The band gaps (in eV) calculated at PBE, PBE+U, and HSE06 levels of theory for the doped and undoped perovskites. The U parameters used for Zr, Ti, or Hf are given in the parentheses.

<b>System</b>	<b>PBE</b>	<b>PBE+U</b>	<b>HSE06</b>	<b>Previous reports<sup>2,29,30</sup></b>
BZS	1.04	1.78 (U = 6.3)	1.81	1.74, 1.8
BZTS (12.5%)	0.94	1.56 (U = 6.0, 6.0)	1.89	~1.40
BZTS (25%)	1.00	1.33 (U = 6.0, 6.0)	1.96	~1.20
BZHS (12.5%)	1.07	1.73 (U = 6.0, 6.0)	1.84	
BZHS (25%)	1.09	1.74 (U = 6.0, 6.0)	1.86	
BZSO	0.95	1.63 (U = 7.0)	1.74	
BZSSe	0.83	1.45 (U = 6.0)	1.46	

#### S4. Unique BZTS (25%) geometries

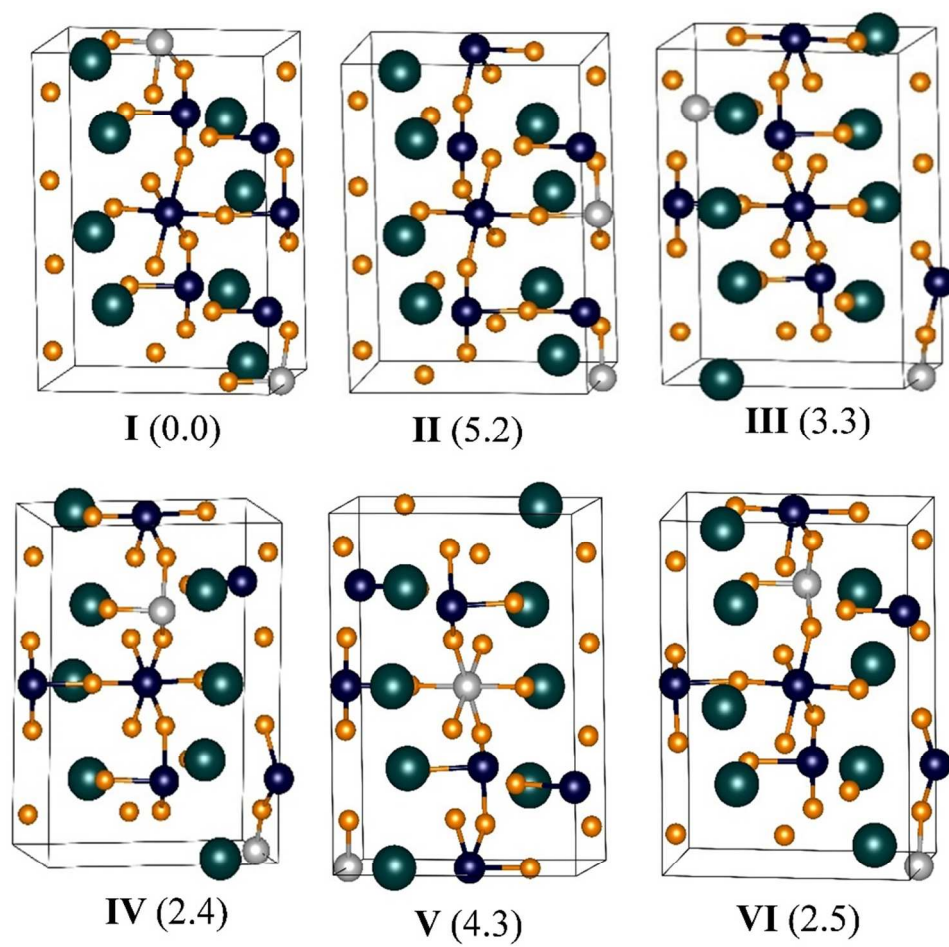


**Figure S1.** Optimized geometries of different configurations of BZTS with 25% Ti doping and their relative energies with respect to the most stable geometry (I).



**S5. Comparison of timescales, NAC, and dephasing times with respect to the active spaces and number of stochastic realization of surface hopping trajectories used for the NA-MD simulations.**

<b>Table S3.</b> Comparison of recombination times, average NAC, and dephasing times with respect to the active space. The values outside the parenthesis represent the results obtained when CBM, VBM, and other band edge states (within an energy window of 5 $k_B T$ ) are included in the active space. The values inside the parenthesis represent the results obtained when only CBM and VBM are included in the active space.			
System	Recombination time, ns	NAC, meV	Dephasing time, fs
BZS	6.84 (9.08)	0.74 (0.74)	30.68 (30.83)
BZTS (12.5%)	0.75 (1.11)	1.30 (1.28)	12.08 (10.90)
BZTS (25%)	0.23 (0.37)	1.66 (1.51)	12.96 (12.94)
BZS	6.84 (9.08)	0.74 (0.74)	30.68 (30.83)
BZHS (12.5%)	5.72 (8.69)	0.96 (0.93)	12.54 (13.49)
BZHS (25%)	5.08 (4.93)	0.79 (0.80)	28.60 (25.02)
BZSO	1.18 (2.01)	1.13 (1.08)	13.97 (14.90)
BZS	6.84 (9.08)	0.74 (0.74)	30.68 (30.83)
BZSSe	3.72 (3.01)	0.65 (0.69)	18.38 (18.85)

<b>Table S4.</b> Comparison of recombination times, average NAC, and dephasing times with respect to the number of stochastic realization of surface hopping trajectories. The values outside and inside the parenthesis represent the results obtained when 200000 and 20000, respectively stochastic realization of surface hopping trajectories are utilized for the NA-MD calculations. In both cases, only VBM and CBM states are included in the active space.			
System	Recombination time, ns	NAC, meV	Dephasing time, fs
BZS	9.08 (4.64)	0.74	30.83 (30.70)
BZTS (12.5%)	1.11 (0.98)	1.28	10.90 (10.90)
BZTS (25%)	0.37 (0.37)	1.51	12.94 (12.95)
BZS	9.08 (4.64)	0.74	30.83 (30.70)
BZHS (12.5%)	8.69 (5.90)	0.93	13.49 (13.50)
BZHS (25%)	4.93 (4.91)	0.80	25.02 (25.02)
BZSO	2.01 (2.46)	1.08	14.90 (14.90)
BZS	9.08 (4.64)	0.74	30.83 (30.70)
BZSSe	3.01 (2.63)	0.69	18.85 (18.85)

**S6. Recombination dynamics in chalcogenide perovskites calculated by employing an active space consisting of VBM, CBM, and other band edge states within an energy window defined by  $> 2.5 k_B T + \text{VBM}$  and  $< 2.5 k_B T + \text{CBM}$ ). 200000 stochastic realization of SH trajectories are considered (20 initial conditions and 10000 stochastic realization of SH trajectories for each initial condition. Timescales are presented in Table 1)**

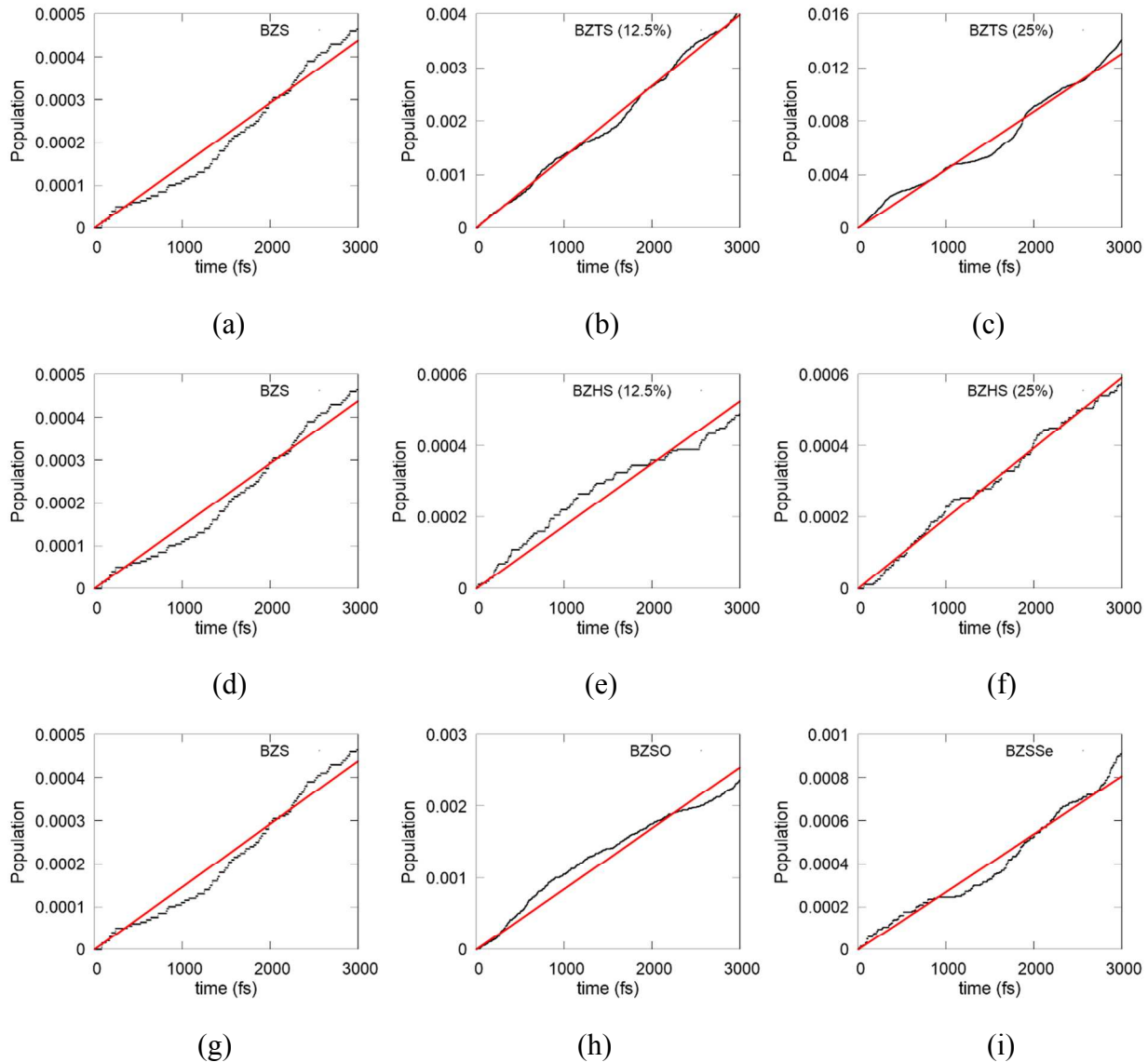
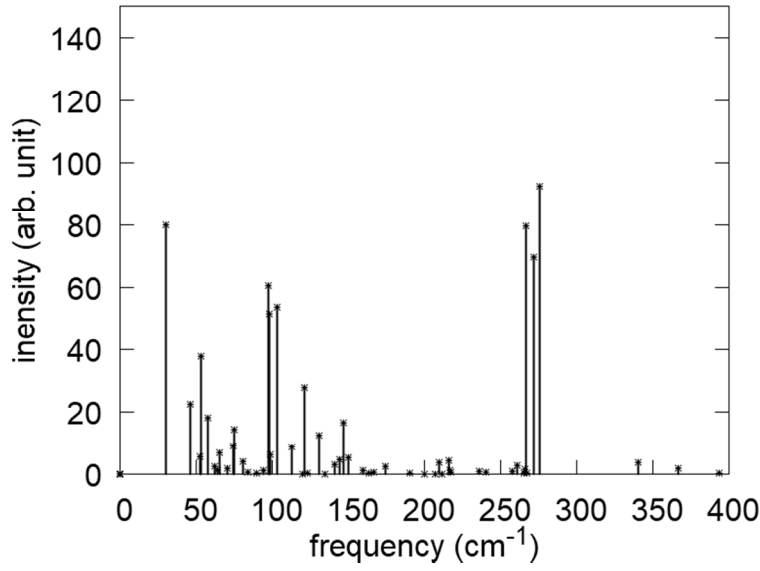


**Figure S2.** Ground state population recovery due to the relaxation of lowest energy excited state and the corresponding exponential fit used to calculate the recombination timescales in (a, d, h)

BZS, (b) BZTS (12.5%), (c) BZTS (25%), (e) BZHS (12.5%), (f) BZHS (25%), (g) BZSO, and

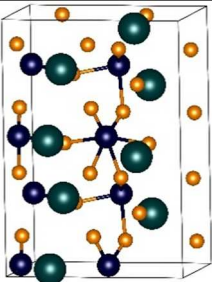
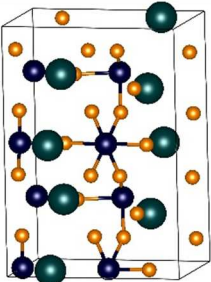
(i) BZSSe. The population data is fitted by the equation  $f(t)=1-e^{\left(\frac{-t}{\tau}\right)}$  where  $\tau$  is the recombination time.

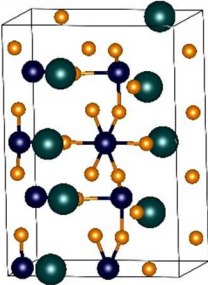
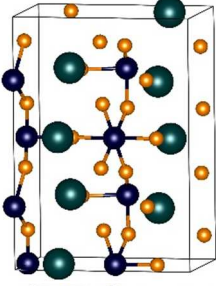
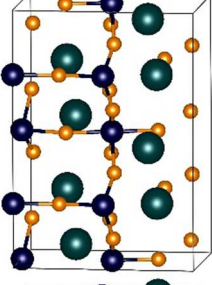
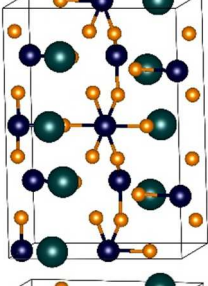
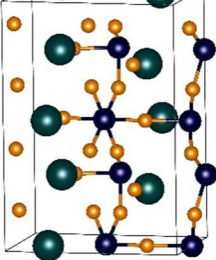
**S7. Phonon (IR active modes) spectrum of BZS at  $\Gamma$  point.**



**Figure S3.** Phonon spectrum of BZS calculated at the  $\Gamma$  point.

**S8. Testing the convergence of energy and computational time with respect to the k-point mesh.**

<b>Table S5.</b> Comparison of optimized geometries, relative energies, and computational time with respect to the k-point mesh used for the calculations of $1 \times 2 \times 1$ supercell of BZS. We used a $3 \times 2 \times 2$ k-point mesh for the MD simulations as it gives the best compromise between the computational time and accuracy.			
<b>K-point mesh</b>	<b>Optimized geometry</b>	<b>Energy, relative to the converged value (eV)</b>	<b>Wall time for single point energy calculation (m)</b>
$1 \times 1 \times 1$		3.32	2.4
$2 \times 1 \times 1$		1.75	3.4

2×2×2		0.23	11.2
3×2×2		0.08	11.2
4×3×3		0.01	24.5
5×4×4		0.00	53.9
7×4×5		0.00	88.0

**S9.** The following input files are attached as part of the supporting information files.

(a) py-scr3.txt - python file for running the NA-MD simulation using PYXAID.

Files (b-m) are Quantum Espresso input files used for the geometry optimization of perovskites structures. Each file contains optimized coordinates and cell-parameters.

(b) BZS.txt - calculations setup for geometry optimization and final coordinates of  $\text{BaZrS}_3$ .

(c) BZSO.txt - calculations setup for geometry optimization and final coordinates of  $\text{BaZrS}_{1.5}\text{O}_{1.5}$ .

(d) BZSSe.txt - calculations setup for geometry optimization and final coordinates of  $\text{BaZrS}_{1.5}\text{Se}_{1.5}$ .

(e) BZHS\_12p5.txt - calculations setup for geometry optimization and final coordinates of  $\text{BaZr}_{1-x}\text{Hf}_x\text{S}_3$  ( $x = 0.125$ ).

(f) BZHS\_25.txt - calculations setup for geometry optimization and final coordinates of  $\text{BaZr}_{1-x}\text{Hf}_x\text{S}_3$  ( $x = 0.25$ ).

(g) BZTS\_12p5.txt - calculations setup for geometry optimization and final coordinates of  $\text{BaZr}_{1-x}\text{Ti}_x\text{S}_3$  ( $x = 0.125$ ).

(h) BZTS\_25.txt - calculations setup for geometry optimization and final coordinates of most stable configuration (I, Figure S1) of  $\text{BaZr}_{1-x}\text{Ti}_x\text{S}_3$  ( $x = 0.25$ ).

(i) BZTS\_25\_II.txt - calculations setup for geometry optimization and final coordinates of configuration II (Figure S1) of  $\text{BaZr}_{1-x}\text{Ti}_x\text{S}_3$  ( $x = 0.25$ ).

(j) BZTS\_25\_III.txt - calculations setup for geometry optimization and final coordinates of configuration III (Figure S1) of  $\text{BaZr}_{1-x}\text{Ti}_x\text{S}_3$  ( $x = 0.25$ ).

(k) BZTS\_25\_IV.txt - calculations setup for geometry optimization and final coordinates of configuration IV (Figure S1) of  $\text{BaZr}_{1-x}\text{Ti}_x\text{S}_3$  ( $x = 0.25$ ).

(l) BZTS\_25\_V.txt - calculations setup for geometry optimization and final coordinates of configuration V (Figure S1) of  $\text{BaZr}_{1-x}\text{Ti}_x\text{S}_3$  ( $x = 0.25$ ).

(m) BZTS\_25\_VI.txt - calculations setup for geometry optimization and final coordinates of configuration VI (Figure S1) of  $\text{BaZr}_{1-x}\text{Ti}_x\text{S}_3$  ( $x = 0.25$ ).

## Author Information

### Corresponding Author

\* Email: [alexeyak@buffalo.edu](mailto:alexeyak@buffalo.edu) Twitter: @AkimovLab

## References

- (1) Clearfield, A. The Synthesis and Crystal Structures of Some Alkaline Earth Titanium and Zirconium Sulfides. *Acta Crystallogr.* **1963**, *16*, 135–142.
- (2) Perera, S.; Hui, H.; Zhao, C.; Xue, H.; Sun, F.; Deng, C.; Gross, N.; Milleville, C.; Xu, X.; Watson, D. F.; et al. Chalcogenide Perovskites – an Emerging Class of Ionic Semiconductors. *Nano Energy* **2016**, *22*, 129–135.
- (3) Perdew, J. P.; Burke, K.; Ernzerhof, M. Generalized Gradient Approximation Made Simple. *Phys. Rev. Lett.* **1996**, *77*, 3865–3868.
- (4) Gianozzi, P.; Baroni, S.; Bonini, N.; Calandra, M.; Car, R.; Cavazzoni, C.; Ceresoli, D.; Chiarotti, G. L.; Cococcioni, M.; Dabo, I.; et al. QUANTUM ESPRESSO: A Modular and Open-Source Software Project for Quantum Simulations of Materials. *J Phys Condens Matter* **2009**, *21*, 395502.
- (5) Shamp, A.; Terpstra, T.; Bi, T.; Falls, Z.; Avery, P.; Zurek, E. Decomposition Products of Phosphine Under Pressure:  $\text{PH}_2$  Stable and Superconducting? *J. Am. Chem. Soc.* **2016**, *138*, 1884–1892.
- (6) Chowdhury, C.; Karmakar, S.; Datta, A. Capping Black Phosphorene by H-BN Enhances Performances in Anodes for Li and Na Ion Batteries. *ACS Energy Lett.* **2016**, *1*, 253–259.
- (7) Karmakar, S.; Chowdhury, C.; Datta, A. Two-Dimensional Group IV Monochalcogenides: Anode Materials for Li-Ion Batteries. *J. Phys. Chem. C* **2016**, *120*, 14522–14530.
- (8) Gross, N.; Sun, Y.-Y.; Perera, S.; Hui, H.; Wei, X.; Zhang, S.; Zeng, H.; Weinstein, B. A. Stability and Band-Gap Tuning of the Chalcogenide Perovskite  $\text{BaZrS}_3$  in Raman and Optical Investigations at High Pressures. *Phys. Rev. Appl.* **2017**, *8*, 044014.
- (9) Heyd, J.; Scuseria, G. E.; Ernzerhof, M. Hybrid Functionals Based on a Screened Coulomb Potential. *J. Chem. Phys.* **2003**, *118*, 8207–8215.
- (10) Anisimov, V. I.; Zaanen, J.; Andersen, O. K. Band Theory and Mott Insulators: Hubbard U instead of Stoner I. *Phys. Rev. B* **1991**, *44*, 943–954.



- (11) Cococcioni, M.; de Gironcoli, S. Linear Response Approach to the Calculation of the Effective Interaction Parameters in the LDA+U Method. *Phys. Rev. B* **2005**, *71*, 035105.
- (12) Hammes-Schiffer, S.; Tully, J. C. Proton Transfer in Solution: Molecular Dynamics with Quantum Transitions. *J. Chem. Phys.* **1994**, *101*, 4657–4667.
- (13) Akimov, A. V.; Prezhdo, O. V. The PYXAID Program for Non-Adiabatic Molecular Dynamics in Condensed Matter Systems. *J. Chem. Theory Comput.* **2013**, *9*, 4959–4972.
- (14) Akimov, A. V.; Prezhdo, O. V. Advanced Capabilities of the PYXAID Program: Integration Schemes, Decoherence Effects, Multiexcitonic States, and Field-Matter Interaction. *J. Chem. Theory Comput.* **2014**, *10*, 789–804.
- (15) Akimov, A. V.; Neukirch, A. J.; Prezhdo, O. V. Theoretical Insights into Photoinduced Charge Transfer and Catalysis at Oxide Interfaces. *Chem. Rev.* **2013**, *113*, 4496–4565.
- (16) Madjet, M. E.-A.; Akimov, A. V.; El-Mellouhi, F.; Berdiyrov, G. R.; Ashhab, S.; Tabet, N.; Kais, S. Enhancing the Carrier Thermalization Time in Organometallic Perovskites by Halide Mixing. *Phys Chem Chem Phys* **2016**, *18*, 5219–5231.
- (17) Akimov, A. V.; Muckerman, J. T.; Prezhdo, O. V. Nonadiabatic Dynamics of Positive Charge during Photocatalytic Water Splitting on GaN(10-10) Surface: Charge Localization Governs Splitting Efficiency. *J. Am. Chem. Soc.* **2013**, *135*, 8682–8691.
- (18) Long, R.; Fang, W.; Akimov, A. V. Nonradiative Electron–Hole Recombination Rate Is Greatly Reduced by Defects in Monolayer Black Phosphorus: Ab Initio Time Domain Study. *J. Phys. Chem. Lett.* **2016**, *7*, 653–659.
- (19) Pradhan, E.; Magyar, R. J.; Akimov, A. V. Scaling Relationships for Nonadiabatic Energy Relaxation Times in Warm Dense Matter: Toward Understanding the Equation of State. *Phys. Chem. Chem. Phys.* **2016**, *18*, 32466–32476.
- (20) Nie, Z.; Long, R.; Sun, L.; Huang, C.-C.; Zhang, J.; Xiong, Q.; Hewak, D. W.; Shen, Z.; Prezhdo, O. V.; Loh, Z.-H. Ultrafast Carrier Thermalization and Cooling Dynamics in Few-Layer MoS<sub>2</sub>. *ACS Nano* **2014**, *8*, 10931–10940.
- (21) Long, R.; English, N. J.; Prezhdo, O. V. Minimizing Electron–Hole Recombination on TiO<sub>2</sub> Sensitized with PbSe Quantum Dots: Time-Domain Ab Initio Analysis. *J. Phys. Chem. Lett.* **2014**, *5*, 2941–2946.
- (22) Tully, J. C. Molecular Dynamics with Electronic Transitions. *J. Chem. Phys.* **1990**, *93*, 1061–1071.
- (23) Mi, Y.; Odaka, H.; Iwata, S. Electronic Structures and Optical Properties of ZnO, SnO<sub>2</sub> and In<sub>2</sub>O<sub>3</sub>. *Jpn. J. Appl. Phys.* **1999**, *38*, 3453–3458.
- (24) Johnson, K. A.; Ashcroft, N. W. Corrections to Density-Functional Theory Band Gaps. *Phys. Rev. B* **1998**, *58*, 15548.
- (25) Gygi, F.; Baldereschi, A. Quasiparticle Energies in Semiconductors: Self-Energy Correction to the Local-Density Approximation. *Phys. Rev. Lett.* **1989**, *62*, 2160–2163.
- (26) Wang, L.; Akimov, A.; Prezhdo, O. V. Recent Progress in Surface Hopping: 2011–2015. *J. Phys. Chem. Lett.* **2016**, 2100–2112.
- (27) Jaeger, H. M.; Fischer, S.; Prezhdo, O. V. Decoherence-Induced Surface Hopping. *J. Chem. Phys.* **2012**, *137*, 22A545.
- (28) Mukamel, S. *Principles of Nonlinear Optical Spectroscopy*; Oxford University Press: New York, 1995.
- (29) Meng, W.; Saparov, B.; Hong, F.; Wang, J.; Mitzi, D. B.; Yan, Y. Alloying and Defect Control within Chalcogenide Perovskites for Optimized Photovoltaic Application. *Chem. Mater.* **2016**, *28*, 821–829.
- (30) Sun, Y.-Y.; Agiorgousis, M. L.; Zhang, P.; Zhang, S. Chalcogenide Perovskites for Photovoltaics. *Nano Lett.* **2015**, *15*, 581–585.

